©Copyright 2019
Dylan S. Reynolds

Evaluating Wind Fields for Use in Distributed Snowpack Models

Dylan S. Reynolds

A thesis
submitted in partial fulfillment of the
requirements for the degree of

Master of Science in Civil Engineering

University of Washington
2019

Committee:
Jessica Lundquist
David Shean

Program Authorized to Offer Degree:
Civil and Environmental Engineering

University of Washington

Abstract

Evaluating Wind Fields for Use in Distributed Snow Models

Dylan S. Reynolds

Chair of the Supervisory Committee:
Professor Jessica Lundquist
Civil and Environmental Engineering

Mountain winds are the driving force behind snow accumulation patterns in mountainous catchments, making accurate wind fields a prerequisite to accurate simulations of snow depth for water resource forecasting. Here we evaluate calculated wind fields using a new method for inferring the wind direction from snow depth patterns. This method leverages established relationships between snow depth and wind direction and provides the dominant wind direction at 260 locations in the Tuolumne River Watershed, CA. We compare these inferred wind directions to wind fields derived from combinations of coarse data and downscaling schemes. Coarse data come from meteorological towers, NLDAS, or HRRR data, and downscaling schemes tested include MicroMet, WindNinja, and bilinear interpolation. All downscaled wind fields replicate the south-west winds suggested by snow-depth-inferred wind directions. We then use these wind fields to force SnowModel, which contains the wind-transport scheme SnowTran. We find that wind fields derived from meteorological observations rarely achieve high wind speeds necessary for wind redistribution of snow. NLDAS data are derived from a 32 km DEM which smooths the Sierra Nevada range and results in low wind

speeds over isolated peaks. Wind fields created by bilinearly interpolating coarse data do not contain discontinuities in wind speed necessary for deposition of snow. Two wind fields derived from 3 km HRRR data and downscaled with respect to terrain produced snow depth maps that best matched observations of snow depth from airborne LiDAR. We recommend 3 km resolution gridded wind data downscaled with respect to terrain as input to distributed snow models.

1. Introduction

Snow provides a reliable water supply to much of the world. This snow melts out according to the pattern of snow distribution built up over the accumulation season [*Anderton et al. 2002*]. During the accumulation season, winds are the primary driver of snow distribution patterns at non-forested sites, or sites in arctic or prairie regions [*Winstral et al. 2002; Luce et al. 1998; Deems et al. 2008; Sturm and Wagner 2010; Pomeroy et al. 1993; Pomeroy et al. 1997*]. Thus, since melt-timing of spring snow is determined by the existing distribution of snow when melt begins [*Lundquist and Dettinger 2005*; *Lundquist et al. 2005*], properly modeling wind processes is a prerequisite to obtaining accurate late-season water forecasts in snow-dominated basins [*Luce et al. 1998*]. The snow hydrology community has embraced this, embarking on a number of studies to properly model wind-transport of snow [*Ohara 2014; Liston et al. 2007; Liston and Sturm 1998; Lehning et al. 2006*]. Other research has focused on what wind fields should be used in these snow transport models [*Wagenbrenner et al. 2016; Beaucage et al. 2014; Musselman et al. 2015*]. These studies often use ground-based observations from meteorological towers to evaluate different wind fields [*Musselman et al. 2015; Gascoin et al. 2013*].

While information about mountain winds can be provided by meteorological stations, they come with some important caveats. Due to the cost of the instruments and the difficulty of accessing remote sites, wind sensors are only found at 36% of Western US meteorological stations that measure snow [*Raleigh et al. 2016*]. Wind conditions are highly variable across a basin, and do not vary according to simple linear relationships. This intense spatial heterogeneity, combined with the difficulties in deploying instrumentation, make it difficult to fully resolve wind patterns based on meteorological observations alone. This results in either under-evaluating wind fields when point observations are used for validation, or under-sampling when point observations are used to create forcing data for distributed hydrologic models.

Observations of environmental processes can either be obtained directly by instrumenting the natural world or indirectly by paying attention to existing clues in the landscape. Natural processes often leave evidence of their action, and this fact is used extensively in fields such as glaciology and geology. Learning to identify patterns in nature can ultimately teach us about the environment that shaped them [*Sturm and Wagner 2010; Grayson and Blöschl 2001*]. As mentioned above, winds are the primary control on snow distribution patterns at some sites. Thus, we hypothesize that snow depth patterns at the end of the accumulation season contain information about the average, snow-transporting winds at a given site.

Prior studies have established relationships between the properties of a site's snow depth distribution and the dominant wind direction at exposed, non-forested sites [*Deems et al. 2006; Trujillo et al. 2009; Mott et al. 2011]*. These relationships show that snow depth distributions entomb information about the winds that shaped them, an idea that is familiar to winter recreationalists and naturalists. We believe that these relationships can be used to augment sparse meteorological observations and allow for more thorough evaluations of calculated wind fields.

Due to the variability of wind fields and the complexity inherent to simulating them at resolutions typical of distributed snow models (< 1km), wind fields for distributed snowpack models are often obtained by downscaling coarse reanalysis data. The snow modeler is then faced with a decision of what coarse dataset to use, and what downscaling method to apply. In this study we evaluate different combinations of coarse datasets and downscaling schemes to determine the tradeoffs of each. Prior studies have shown that evaluating wind fields at points can lead to different results than evaluating them based on their ability to drive wind-

redistribution in distributed snowpack models [*Musselman et al. 2015*]. Thus, in addition to a point comparison of wind fields, we evaluate these downscaled wind fields by running a distributed snowpack model and comparing output to observations from airborne LiDAR.

In section 2 we review observations of wind-redistribution of snow and models of wind-related snow transport to determine what features of wind fields are most important when modeling wind-redistribution. In sections 3 and 4 we profile a variety of coarse wind datasets and downscaling schemes used to generate wind fields. Then in section 5, we introduce a new technique for inferring the dominant, snow-transporting wind direction at sites where wind observations do not exist. In sections 6 and 7 we use the inferred wind directions, along with a series of snow model runs, to determine how these wind fields differ and what effect these differences have on modeling snowpack. We conclude with recommendations in section 8, advocating the use of gridded wind data downscaled with respect to terrain.

2.0 Background

2.1 Processes of wind-redistribution of snow

Wind-redistribution of snow occurs when the surface shear velocity exceeds some value necessary for wind-redistribution to begin. This value, which must be exceeded for transport, is referred to as the threshold shear velocity. Previous studies have observed the threshold shear velocity in wet snow environments to be between 0.38 m s^{-1} and 0.76 m s^{-1} at the ground surface [*Li and Pomeroy 1997*]. This threshold speed determines both if wind-redistribution can occur, and how much snow can be transported when it does [*Schmidt 1982*]. In the environment, the threshold velocity that determines when wind-redistribution occurs is not constant. It will increase as the snow surface sinters and bonds between snowfall events, and drop when fresh, light snow is deposited on the surface during snowfall.

Once redistribution occurs, there are three primary mechanisms by which wind interacts with the snowpack. Snow can undergo saltation, where grains are bounced along the snow surface within 0.1 m of the surface. Snow can also undergo suspension, where it is entrained in the flow by turbulent eddies and carried meters above the surface. Snow transported via suspension can travel up to hundreds of meters before being deposited [*Mott et al. 2018*]. Observations of the transport rate of snow via winds agree on an exponential increase in mass flux with increasing wind speeds [*Nishimura and Nemoto 2005; Schmidt 1982; Pomeroy and Male 1992*]. Both saltation and suspension cause snow grains to have more contact with the atmosphere along their surface. Depending on the temperature and humidity, this can lead to enhanced sublimation of the snow grains compared to sublimation of the static snow surface.

Different fields of study have different conventions for reporting wind direction. In this study we refer to all wind directions as the direction from which the wind originated. For example, a wind direction of 0º indicates a wind that is blowing from the north and to the south. In this study we use term “wind transport” to refer to any effect that winds have on the distribution of snow. Wind-redistribution, however, refers only to wind-transport of snow that occurs after the snow has been deposited, such as saltation and suspension [*Mott et al. 2018*]. Because these are the only two processes of wind-transport modeled in SnowTran and examined in this study, we use the term wind-redistribution. Lastly, we define the term “snow drift” as any snow feature caused by wind-transport of snow.

2.2 Existing methods of calculating wind-redistribution

To examine how the snow modeling community tends to represent these processes, we review the equations for wind-redistribution of snow in two well-cited models: SnowTran, which is used in SnowModel, and the Prairie Blowing Snow Model (PBSM). Other wind-transport models which use more physically explicit, computationally intensive equations of transport are excluded from this review since they are not suited to model snow over the large domain used in this study. These two models use almost identical equations to calculate the rate of transport via saltation. PBSM considers the effects of exposed vegetation in its calculation of saltation [*Pomeroy et al 1993*]. Assuming a snow depth greater than vegetation height, however, these two estimates of saltation become identical. The two models also feature identical methods for calculating the sublimation of blowing snow, with the authors of SnowTran stating that, "Our formulation for the sublimation rate of wind transported snow […] follows that of Schmidt (1972, 1991), [and] Pomeroy and others (1993)" [*Liston and Sturm 1998*].

The primary difference between these two models comes in their calculation of transport via suspension. SnowTran's suspension equation leads to 1-2x more transport via suspension than predicted by the *Pomeroy and Male 1991* formulation used in PBSM. Still, both methods scale snow transport by suspension exponentially with respect to wind speed, with the PBSM model transporting 90% of snow via suspension for surface shear speeds of 0.92 m s^{-1} [*Pomeroy and Male 1992*]. For the scope of this review, we simply note this agreement on the exponential relationship of suspension transport rate to wind speed and continue a more detailed comparison of the two suspension schemes in section 7. Due to the exponential nature of this relationship, we note that both models are dependent on the distribution of wind speeds, particularly the maximum wind speeds and their frequency of occurrence.

SnowTran was updated in 2007 to include a variable threshold shear speed [*Liston et al 2007*]. During precipitation events the threshold shear speed decreases. As a result, any winds during precipitation events are more likely to cause snow transport and to cause significant amounts of snow transport than a similar wind event not during a precipitation period. This means that in SnowTran and models with similar variable threshold shear speeds, the timing of wind speeds is important.

Lastly, both models calculate the change in snow depth over a grid cell by determining the change in snow-transport flux for the cell. This follows from requiring a conservation of mass for the grid cell. For example, if a significant amount of snow is leaving the cell via saltation and none is coming in, the cell will experience a decrease in snow depth. Because these flux terms, and particularly suspension flux, are dependent on the wind speed, SnowTran and PBSM depend on spatial discontinuities in the wind speed field to allow for the deposition of snow. If these changes in transport flux do not occur, the snow will remain in the atmosphere longer, where it is more likely to sublimate.

2.3 Desired qualities in wind fields

The two methods for estimating wind-transport of snow reviewed above share a few key similarities: exponential increase in wind-transport of snow with increasing wind speeds, primary transport via suspension at high wind speeds, and spatial discontinuities in the wind speed field leading to deposition. SnowModel also features a varying threshold shear speed, which adds

importance to the timing of high-wind events relative to precipitation events. We also find it necessary to state the obvious, that in both models the direction of winds is critical to determining the pattern of snow caused by wind redistribution. From this review, we arrive at four characteristics of wind fields deserving of consideration. These are 1) direction of winds, 2) frequency of high wind speeds, 3) spatial heterogeneity of wind speeds, and 4) timing of high wind events relative to snowfall. In sections 6 and 7 we will discuss the performance of different wind fields in terms of these characteristics.

3.0 Location and Data

3.1 Site Description

This study focuses on the upper Tuolumne watershed in Yosemite National Park, California. This region encompasses large, subalpine meadows, peaks nearly 4000 m above mean sea level (MSL), and narrow valleys and canyons. Tree-line occurs around roughly 3000 m MSL, and much of the domain is comprised of bare expanses of granite. This limited vegetation cover makes the domain desirable for modeling both snowpack and winds. Interception of snow by vegetation complicates simulations of snowpack evolution, while the interaction of vegetation with winds leads to complex, fine-scale structures in the wind field. To evaluate the technique for inferring wind direction presented in section 5.1, we chose 9 sites around this domain with different site properties. Four of the sites are below tree-line and contain either sparse trees or extensive forest cover. Two of the sites are above tree-line and contain deep granitic fissures, which are discussed in-depth in section 6.1. The remaining three sites, Kuna_North, Meadows_Ridge, and Doghead_Peak, are above tree-line, are identified in Figure 1, and will be discussed in sections 6 and 7.

3.2 LiDAR Data

The upper Tuolumne basin was chosen both due to its varied terrain, and the availability of distributed snow depth data from NASA's ASO program [*Painter et al. 2016*]. ASO snow depth data were obtained from LiDAR measurements by differencing a snow-on flight from a bare-earth, snow-off flight. Airborne LiDAR data has been found to properly capture the spatial variability of snowpack when compared to manual transects at open and forested sites [*Currier et al. 2019*].

In this study we use 3-m snow depth data from WY2017. To infer the dominant wind direction as described in section 5.1, snow depth data from the earliest flight, 3 March 2017 were used. This is done in order to minimize melt patterns and maximize accumulation patterns by wind redistribution. When comparing SnowModel output with observations of snow depth in sections 6 and 7, the 1 April 2017 flight was used.

3.3 HRRR data

10 m U- and V-component wind speeds from the High-Resolution Rapid Refresh (HRRR) model were used to generate three of the wind fields in this study [*Benjamin et al. 2015*]. HRRR was chosen because it provides high-resolution spatial and temporal output for a well-studied weather model, WRF [*Hovarth et al. 2012*]. We used the University of Utah's HRRR archive (http://hrrr.chpc.utah.edu/) [*Blaylock et al. 2017*]. HRRR runs the Weather Research and Forecasting (WRF) model for its physical calculations and assimilates a variety of high-resolution hourly observations from radar and satellites. The model provides data at a 3 km scale over the continental US at an hourly time step. This model resolution means that HRRR uses a 3 km DEM for its domain, which has important implications for modeling winds. We also used HRRR temperature, precipitation, and relative humidity variables to force all SnowModel runs discussed in section 4.2. The script used to pull and subset HRRR data from the archive can be found here: (https://github.com/d-reynolds/HrrrPy).

3.4 NLDAS data

The North American Land Data Assimilation System (NLDAS) dataset has been used in many prior snow studies (e.g., *Margulis et al. 2016*), so we also include its wind data in this study. Again, 10 m U- and V-component wind speeds from NLDAS are used to generate wind fields. The NLDAS dataset obtains its wind data from the North American Regional Reanalysis (NARR) model [*Xia et al. 2012*]. NARR outputs variables at a 32 km grid spacing, meaning that it resolves the terrain at this resolution. 32 km NARR wind data are bilinearly interpolated to the approximately 12.5 km grid size used by NLDAS.

3.5 CDEC data

Another source of wind data were three meteorological stations distributed throughout the study domain (Figure 1). Stations included in this study use mechanical anemometers to measure 10 m wind speed and direction at their sites. These data were chosen since meteorological observations from towers are a common source of forcing data for snow models. These data were obtained through the California Data Exchange (CDEC). Wind data at these stations are sampled sub-hourly and averaged to hourly observations of wind speed and direction. These three stations were chosen because they have records of wind speed and direction throughout WY2017. As noted in section 1, meteorological stations are prone to damage due to the harsh environment in which they operate, and not all stations in the study domain were reporting data during WY2017. If one of the three sensors used reported a lapse in observations, no correction was made, and the downscaling scheme applied simply distributed observations without this point. We believe that this allows for a fair comparison of the accuracy of data and quality of data among the wind fields tested. Approximately 4% of the wind sensor record contained gaps in observations.

4.0 Models

4.1 Downscaling models

Two wind-downscaling models, MicroMet and WindNinja, were used to downscale the 3 wind datasets outlined above to a resolution of 150 m. MicroMet (MM) is a meteorological interpolation scheme developed as a preprocessing step to the snow model, SnowModel [*Liston and Elder 2006*]. In MicroMet, wind speed and direction are first interpolated to a finer grid from the coarse forcing data. Then, wind speed and direction are adjusted depending on the topographic slope and curvature at a given grid cell. MicroMet was chosen due to its relative simplicity of calculation, and widespread use in the snow modeling community [*Pflug et al. 2019; Bernhardt et al. 2010; Gascoin et al. 2013; Currier and Lundquist 2018*]. While MicroMet wind speeds have been evaluated over confined areas with dense points of observation [*Liston and Elder 2006*], it has seen fewer evaluations of wind speeds over entire modeling domains [*Gascoin et al. 2013*], or evaluations of wind direction.

Instead of interpolating using empirically-derived equations as MicroMet does, winds can also be downscaled using more physical-based models. We chose WindNinja as a more physically based model that is not prohibitively computationally demanding. WindNinja 3.5.0 (WN) is a wind-downscaling model developed by the US Forest Service to be used operationally during forest fire management. It features a mass-conservation solver that modifies the initial wind field by minimizing change from the input vectors, while maintaining zero divergence in the wind field [*Forthofer et al. 2014*]. This model is more computationally expensive than MicroMet but can still downscale months of coarse wind data in a couple days on a personal laptop.

Lastly, bilinear interpolation alone was used as a downscaling scheme due to its simplicity of implementation. These three downscaling methods, when applied to the HRRR, NLDAS, and CDEC data, represent a spectrum of wind fields ranging in computationally intensity. In this way we hope to demonstrate trade-offs between wind fields and determine if more computationally intensive methods are justified by an increase in the accuracy of modeled winds.

4.2 Simulations with a distributed snow model

Point-evaluations and distributed-evaluations of wind fields can yield different conclusions about the accuracy of the wind fields tested [*Musselman et al. 2015*]. To fully vet the wind fields, we ran six different simulations of the distributed snow model, SnowModel, for WY2017 [*Liston and Elder 2006*]. The model was run at 150 m resolution over the domain shown in Figure 1. The 3-meter snow-off LiDAR data from the ASO campaign was supplied to the model as a DEM, while NLCD land cover data was used to determine vegetation type [*Yang et al. 2018*]. The six different simulations and their configurations are shown in Table 1. For all simulations, temperature, relative humidity (RH), and precipitation come from the HRRR model. In model runs with “HRRR” in the name, the wind direction and wind speed are derived from the HRRR model. Model runs named differently have wind data derived from either the NLDAS or CDEC datasets.

The snow depth output from SnowModel on 1 April 2017 was compared with the 1 April 2017 snow depth observations from NASA's ASO program [*Painter et al. 2016*]. It is worth noting that SnowModel contains the submodules MicroMet and SnowTran. MicroMet is the same downscaling scheme discussed in section 4.1, while SnowTran was covered earlier in section 2.2. For a number of the simulations, SnowModel's MicroMet downscaling scheme was not applied to the input wind field, and this is noted in Table 1 when done.

In the process of modeling snow transport using SnowTran, we discovered an error in its calculation of transport near forest edges. For non-forested grid cells downwind of a forested grid cell, modeled surface wind shear speeds increase substantially. This results in the initiation of wind-redistribution at this cell. Since little or no wind transport of snow occurs in the sheltered, forested cells upwind, there is little snow flux into the non-forested grid cell. Thus, there is a net loss of snow from these cells downwind of forest stands. This behavior is to be expected in reality for some point downwind of forest stands. However, for a simulation using discrete grid cells, this point can only be the nearest downwind grid cell, which covers a 150m x 150m area. Thus, large swaths of the simulation report an erroneously large net scour of snow. To compensate for this, we have masked out the first non-forested grid cell immediately downwind of forested grid cells in the results presented. Performing this masking may bias our simulations towards higher snow depth values, but it allows us to compare the distributions of snow depth values from SnowModel output with observations.

5.0 Inferring Wind Directions

5.1 Wind direction from correlation analysis

Spatial autocorrelation is a technique that describes how similar a 2D pattern, or raster, is to itself at different displacements. For example, if two identical, standardized rasters are overlaid and no displacement is made between their positioning, the two rasters are said to have a correlation of 1, the highest possible value. If the pattern contained in the raster is entirely random, the correlation of the two rasters should drop off considerably as the displacement, or lag-distance, increases, regardless of the direction of displacement. If instead the raster contains some features oriented along a particular direction, the correlation will remain high when displacement occurs along this direction (Figure 2.1b). Snow drifts which form on the lee side of topographic features are an example of patterns which contain directional features.

Spatial autocorrelation can be applied to patterns of snow depth, with the presence of anisotropic structures in the autocorrelation function suggesting the presence of snow drifts at the site [*Mott et al. 2011*]. *Trujillo et al. 2009* and *Mott et al. 2011* found that when anisotropies are present in the snow depth autocorrelation function at a site, the dominant snow-transporting wind direction at the site is oriented perpendicular to the anisotropy.

Over a 500m x 500m site we compute the 2D autocorrelation function of snow depth as illustrated in Fig. 2.1a-c. 3m resolution LiDAR data was used for both snow depth and elevation data, and each 500m x 500m raster was standardized by subtracting its mean and diving by its standard deviation. The Wiener-Khinchin Theorem was used to compute both the cross-correlation and autocorrelation functions. Taking the directions perpendicular to the anisotropy yields two possible candidates for the dominant wind direction, both separated by 180º (Figure 2.1d). To determine which of the two directions is the actual dominant wind direction, we

compute the cross-correlation function between 500m x 500m rasters of snow depth and terrain. This is done to tease out which side of the terrain the snow drift has formed on. Snow drifts appear as local maxima in the snow depth distribution, and drifts formed via advection occur downwind from local maxima in the terrain. Thus, in the cross-correlation function between snow depth and terrain, displacements of the terrain raster downwind will increase correlation until the maxima of both patterns overlap (Figure 2.1f). To find this direction, we first compute the gradient of the cross-correlation function between snow depth and terrain (Figure 2.1g).

$$Grad_{CC} = \nabla\Big(Cross\ Correlation\big(DEM, Snow_{Depth}\big)\Big) \quad (1)$$

We then sum all of the gradient vectors, finding that the direction of the resultant vector points towards the lee-side of terrain features. We refer to this vector as the "lee-side vector". Finally, we identify the true wind direction from the two possible candidates as the direction with the larger dot product between itself and the lee-side vector (Figure 2.1h).

There are a couple important assumptions used in this technique. First, if there is no strong anisotropy in the snow depth autocorrelation function, we assume that there are no drifts present. Second, we assume that any anisotropy is caused by wind and no other forces, such as avalanching or differential shading from solar radiation. For the sites shown in Figure 1, we have examined the local topography and determined this to be true. Lastly, we prescribe a single dominant wind direction at each site, instead of allowing for multi-modal distributions of snow-affecting wind directions.

The technique described is used with 3 m resolution airborne LiDAR data, and the cross-correlation is taken between terrain and snow depth. In areas where LiDAR data are unavailable, snow depth maps may be derived from satellite data using structure-from-motion [*Shean et al. 2016*]. This could allow for the inference of wind direction in places like High-mountain Asia where few other observations exist. Finer resolution LiDAR could resolve other patterns of wind-redistribution that do not show up in 3-m LiDAR data (sastrugi, barchans, drifting around tree trunks, etc.) [*Filhol and Sturm 2015*]. Additionally, the cross-correlation could be taken between snow depth and vegetation height or snow depth scans of two different dates. The gradient of these cross-correlation functions would again indicate the direction of wind-drifts relative to some obstacle (vegetation, existing snow drifts). We hope that as sub-meter LiDAR data becomes more ubiquitous, this technique will find a wider range of applications.

5.2 Thresholds used in correlation analysis

When finding the lee-side vector, we sum the vectors in the gradient of the cross-correlation function and take the magnitude of the resultant vector. This magnitude of the summed vector is then compared to the sum of the magnitudes of each vector in the gradient field.

$$\frac{|\Sigma(Grad_{CC})|}{\Sigma(|Grad_{CC}|)} \quad (2)$$

If the magnitude of the lee-side vector is greater than 60% of the sum of the magnitude of all vectors, we conclude that the gradient of the correlation function does represent the direction of drift formation. If the magnitude of the summed vector is not greater than 60% of the magnitude of the summed vectors, the gradient of the correlation function does not strongly agree on a singular direction. This could be due to snow piling up evenly on both sides of terrain features, or snow deposits in granitic ravines that appear as snow drifts in the autocorrelation analysis. Such a case involving granitic ravines is shown in Figure 2.2. Here anisotropies are found in the autocorrelation function, but the gradient of the cross-correlation function does not converge toward a single direction. This suggests that drifts are not forming on a particular side of terrain features, and the deduction of a single dominant wind direction is not possible. The threshold ratio of 60% was determined by comparing the cross-correlation functions of the nine sites tested. This threshold value was chosen conservatively. Sites with prominent wind drifts, such as the one shown in Figure 2.1, report ratios ranging from 75-99%, while the site shown in Figure 2.3 has a ratio of 11%.

Figure 2.3 illustrates another case where the technique cannot infer the wind direction. Anisotropies in the autocorrelation function are found by taking radial transects of the function. If a transect has a mean value greater than 0.4, it is considered to be an anisotropy. The transect with the highest mean value at a site is taken to be the dominant anisotropy. This threshold value of 0.4 was determined by comparing the autocorrelation functions at nine sites that did or did not visually feature anisotropies. This threshold value of 0.4 was chosen conservatively to exclude sites without clear drifting. Sites which exhibit large snow drifts, such as the one shown in Figure 2.1, have anisotropies with mean values ranging from 0.5-0.88, while sites such as the one shown in figure 2.3 have no transects with mean values greater than 0.2. Figure 2.3 shows the process for a site that does not feature a snow drift. After failing to find a transect of the autocorrelation function with a mean value > 0.4, the algorithm stops, concluding that snow drifts do not exist at this site. The site shown in figure 2.3 is a forested site, and prior studies found that anisotropies in the autocorrelation function due to wind were not found at forested sites [*Trujillo et al. 2009*]. The general pattern of inferred wind directions from the south-west shown in Figure 3 did not appear sensitive to small changes (+/- 0.1) of these threshold values. The number of sites at which the wind direction can be inferred did change, but the overall distribution did not. Future work may wish to investigate a more robust thresholding method.

5.3 Comparing wind fields using inferred wind direction

Using correlation analysis to infer wind direction gives us an estimate of what net wind direction shaped the snow depth distribution at a site. This snow pattern has built up over the season and is likely not attributable to one hour during the entire season. To overcome this, we find the modeled dominant direction (MDD) of winds at each of the 500m x 500m sites over which wind direction can be inferred. To find the MDD, we first take all of the modeled winds when wind speed is greater than 7 m s^{-1}. This threshold represents the wind speed at which wind-redistribution of snow is initiated under wet snow conditions [*Li and Pomeroy 1997*]. We then sum all of the hourly wind vectors exceeding this threshold speed, obtaining a resultant vector that represents the cumulative effect of winds at a site. The direction of this resultant vector gives us the MDD, representing the modeled wind direction most responsible for snow transport at the site.

6.0 Results

6.1 Performance of correlation technique

To closely evaluate the technique discussed in section 5.1, we first inferred the wind direction at 9 sites throughout the upper Tuolumne watershed. Of these sites, the technique worked in full at three of the nine, Kuna_North, Meadows_Ridge, and Doghead_Peak. These sites are characterized as being high-elevation ridgelines clear of large evergreen trees. They feature late-season snow drifts identifiable in satellite imagery in August 2017 (Figure 1). At these three sites, we find that the inferred dominant wind direction points in the direction which the observed snow drifts suggest. Two of the nine sites tested showed anisotropic features in the auto-correlation function of snow depth, but the gradient of the cross-correlation function failed to converge on a singular direction. Physically, this means that long, linear, drift-like features are present in the snow depth at these sites, but that there is no single directional relationship between these features and the surrounding topography. Both of these sites featured long and narrow granitic fissures, which are known to occur in the Tuolumne Intrusive Suite [*Riley and Tikoff 2010; Becker et al. 2014*]. These fissures accrue deep deposits of snow from sloughing, shading, and preferential deposition, so the resulting snow depth features are not due exclusively to wind-redistribution processes. The inferred-direction technique also indicated no drifts at four sites below tree-line and featuring extensive vegetation. This result is in line with findings of previous studies which applied correlation techniques to snow depth in vegetated areas [*Trujillo et al. 2009; Deems et al. 2006*]. This analysis at the 9 sites demonstrates that the technique works where expected (non-vegetated ridgelines) and properly identifies areas where large snow drifts are not present (vegetated sites).

After inferring the direction at these 9 sites with known characteristics, we ran the algorithm across the domain shown in Figure 1 by evenly dividing it up into 500 x 500m scenes. The algorithm took 5 minutes to run over a domain of this size, inferring the wind direction at 260 sites in the basin. This is compared to the 3 wind sensors reporting wind direction in the basin during WY2017. The distribution of inferred wind directions shows that most snow-transporting winds come from the south-west (Figure 3), which corresponds to the dominant winter storm-track for the basin [*Lundquist et al. 2015*]. Table 2 shows the characteristics of sites where the wind direction could and could not be inferred.

6.2 Evaluation of modeled wind directions

We find that all three of the wind fields which are derived from HRRR winds represent the distribution of inferred wind directions across the basin (Figure 3). The downscaled winds derived from NLDAS data have a narrower distribution than the inferred wind directions, as can be said of the winds derived from CDEC data. We find that wind fields derived from different coarse datasets report different distributions of wind direction. Wind fields derived from the same coarse dataset but downscaled differently report similar distributions of wind direction. This demonstrates that the choice in coarse wind data has a greater impact on wind direction than what downscaling scheme is applied. However, it is worth noting that once the MicroMet

downscaling scheme is applied, both the NLDAS and CDEC wind direction distributions are consistent with the distribution of inferred wind directions.

6.3 Spatial differences of modeled wind direction

For every cell in the domain, the dot product between two downscaled wind vectors was computed. When wind vectors did not overlap exactly, the dot product was taken between a wind vector from one wind field and the closest wind vector in the second wind field. The mean of these dot products was then taken for each time step in the WY2017 record to obtain the maps displayed in Figure 4. Comparing this map with the topographic information of the domain, we see that the WindNinja and MicroMet schemes disagree most in narrow valleys. Comparing among wind fields with the same downscaling scheme (MicroMet) and different coarse datasets, we find that differences also occur primarily in low-elevation regions. In some areas, wind fields showed differences in modeled wind direction greater than 90º. Disagreements between wind fields from the same downscaling scheme but different coarse datasets also appear greater than disagreements between wind fields from different downscaling schemes but the same coarse datasets. This agrees with the results found in section 6.2.

6.4 Distribution of wind speeds in downscaled wind fields

To compare the distribution of wind speeds generated by different wind fields, we examine a point on Kuna Crest and look at the wind speed values reported here by all SnowModel simulations during WY2017. This point is chosen because it is at an exposed location where wind field differences are exaggerated for demonstration, and where wind-transport of snow is expected to be significant. The CDEC+MM wind field features a sharp peak around 1 m s^{-1}, with only 48% of observations above 1 m s^{-1} over Kuna Crest (Figure 5a). The peak around 1 m s^{-1} is imposed by MicroMet, which sets a minimum wind speed of 1 m s^{-1} to ensure computational stability. The CDF of CDEC+MM wind speeds shows that besides this low peak, the tail of the distribution stretches out to a maximum wind speed of 36 m s^{-1} (Figure 5a).

We find that the NLDAS+MM simulation reports higher wind speeds than the HRRR+Interp simulation at this point (Figure 5a). These differences in wind speeds arise primarily from the downscaling schemes used. Non-downscaled NLDAS data typically reports lower wind speeds than non-downscaled HRRR data. This occurs because the NLDAS dataset derives its wind speeds from 32km NARR data, which is then interpolated to the 12.5 km NLDAS grid. Using a 32 km DEM to represent the complex terrain of the Sierra Nevada results in smoothed terrain, over which speed-up of winds is expected to be low. However, applying the MicroMet downscaling scheme to NLDAS data allows wind speeds to be increased over terrain convexities, somewhat compensating for the low-resolution DEM used by NLDAS. The bilinear interpolation scheme used in the HRRR+Interp simulation results in wind speeds between HRRR nodes that will never exceed the wind speeds at the HRRR nodes themselves. This is simply a function of bi-linear interpolation. This demonstrates how downscaling schemes using only interpolation limit wind speeds to the maximum speed reported by the coarse forcing data. In short, low-resolution gridded data passed through a terrain-conscious downscaling scheme provides better model forcing data than high-resolution gridded data downscaled through interpolation alone.

Lastly, both the HRRR+MM and HRRR+WN wind fields show wind speed distributions skewed toward higher speeds compared with the other wind fields. The HRRR+WN wind field produced the distribution of wind speeds most skewed toward higher speeds of all of the wind fields tested. The HRRR+WN wind field also featured the highest peak speeds of all of the wind fields tested, reporting maximum speeds of 54 m s^{-1} compared to the HRRR+MM wind field's maximum speeds of 34 m s^{-1}.

6.5 SnowModel simulations

6.5.1 SnowModel snow depth patterns

Running SnowModel under the six different configurations demonstrates the necessity of terrain-modified wind data and wind-redistribution processes when modeling snowpack. Comparing SnowModel snow depth output to ASO data on 1 April 2017, we find that the configuration without wind-redistribution (HRRR+NoTran) fails to capture the scour and deposition patterns along the ridgeline of Kuna Crest (Figure 7). We find that the setup forced with bilinearly interpolated HRRR data simulates windward regions of scour seen in the ASO data. However, the HRRR+Interp simulation does not then create regions of deposition and increased snow depths on the leeward side of the ridge. The HRRR+MM and HRRR+WN simulations do capture the general pattern of wind redistribution seen in the ASO snow depth data. We find that the HRRR+WN-forced simulation transports more snow onto the leeside of the ridge than the HRRR+MM -forced simulation, scouring more snow from the windward side as well (Figure 7 and 8). The CDEC+MM and NLDAS+MM simulations both feature a positive bias in snow depth on the windward side of Kuna Crest, and generally show little signs of wind-redistribution (Figure 7 and 8). We observe that the NLDAS+MM, CDEC+MM, HRRR+Interp, and HRRR+NoTran configurations are unable to capture the heterogeneity of snow depth over Kuna Crest (Figure 8). This is compared to the MM+HRRR and WN runs, both of which better reflect the heterogeneity of snow depth seen in the ASO data (Figure 8).

Examining the biases of these six configurations across the whole basin, we find that the HRRR+NoTran simulated snow depth has a positive bias of 19 cm relative to ASO snow depth, indicating that the HRRR+NoTran simulation accumulated more snow than observed (Table 3). The CDEC+MM and NLDAS+MM simulations had biases in snow depth of 28 cm and 11 cm, respectively. The HRRR+Interp SnowModel simulation reported a negative bias of -21 cm, while the HRRR+MM and HRRR+WN simulations had negative biases of -16 and -24 cm, respectively. When examining the biases across a smaller subset of the domain, Kuna Crest, the bias of the NLDAS+MM simulation more than doubles to a bias of 25 cm. For an explanation of this apparent change in performance, we refer the reader to section 7.3.3.

6.5.2 SnowModel transport rates

SnowModel initiates saltation and suspension processes once the surface shear velocity exceeds the threshold shear velocity [*Liston and Sturm 1998*]. Thus, differences in wind-transport of snow can be partly explained by the number of times the surface shear velocity exceeds the threshold velocity. We find that the HRRR+WN and HRRR+MM simulations had the highest domain-averaged percentage of exceedance for the ensemble (Table 3). The CDEC+MM simulation, which had the lowest amount of wind-redistribution of the ensemble,

has the lowest exceedance percentage. This is due to the CDEC forcing data having mostly low values for wind speed (5% exceedance of 2.7 m s^{-1} over Kuna Crest, Figure 5a). Thus, the CDEC+MM simulation failed to resolve the wind-redistribution of snow seen in the HRRR+WN and HRRR+MM simulations simply due to biased-low wind speeds. We attribute this bias to the CDEC stations being located at lower elevation sites sheltered by terrain and vegetation.

As discussed in section 2, SnowTran calculates wind-transport of snow exponentially with respect to surface shear speeds (Figure 5b). Thus, small differences in wind speed, especially at high values, can result in large differences in wind-transport of snow. Applying this to the distribution of wind speeds discussed in section 6.4, we find that simulations with wind speed distributions skewed low (NLDAS+MM, CDEC+MM, HRRR+Interp) had low rates of wind-redistribution (Table 3). Contrasting this, simulations with higher rates of wind-redistribution (HRRR+MM, HRRR+WN) had distributions of wind speed skewed towards higher values.

SnowTran also truncates 10-m wind speeds greater than 30 m s^{-1} to ensure computational stability in the calculation of surface roughness. This truncation significantly affects the HRRR+WN wind field, which reported winds up to 65 m s^{-1} over the basin. Since transport is computed exponentially with respect to wind speed, the HRRR+WN simulation would have resulted in greater rates of wind-redistribution than reported in Table 3 without this truncation of speeds greater than 30 m s^{-1}. In Figure 5a, we report the 10-m wind speeds as ingested by SnowModel, and in Figure 5c, we report the surface shear velocities used in computation of wind-redistribution, which have the 30 m s^{-1} truncation applied.

7.0 Discussion

7.1 Applicability of correlation technique

The technique of inferring wind direction described in section 5.1 was found to work well at non-forested sites with median slopes between 20º and 40º. The technique's poor performance at forested sites is expected given the findings of prior studies [*Trujillo et al. 2009; Mott et al. 2011*]. The technique depends upon finding an anisotropy in snow depth autocorrelation that persists over lag-distances of > 30 m, and these prior studies found that forested sites do not exhibit this. The tree-line in this basin is around 3000 m, and the mean elevation of sites where the wind direction could be inferred was 3100 m (Table 2). Lastly, we see that the technique works best at sites with a median slope between 20-40º, with almost no success at sites with median slopes greater than 40º. This is likely because some terrain irregularities are required to form snow drifts, but sites with slopes > 40º do not retain enough snow to form a drift downwind of terrain.

There are a few caveats to the method. First, we assume that any strong gradient in the cross-correlation of terrain with snow depth is caused by wind-transport of snow. However, avalanches or shading of snow patches on the north side of slopes will also result in some dominant direction in the gradient of the cross-correlation function. It is possible that cornice-triggered avalanches still indicate the local wind direction since they occur on the leeside of a corniced ridge, but such an investigation is beyond the scope of this paper. The technique described here also assumes that, when a snow drift is detected at a site, the winds causing it are perpendicular to the anisotropy in snow depth autocorrelation. In reality, a variety of wind

directions having components perpendicular to a given terrain feature can result in a lee-side snow drift. With the data available in this study, the best estimate that can be made is a direction perpendicular to the snow depth anisotropy.

Lastly, the domain over which the wind direction is inferred needs to be chosen with care. One can imagine a snow drift on the leeward side of some ridge, A, with a nearby adjacent ridge, B, that did not form this snow drift. Using our 500m x 500m windows, we could include the snow drift and ridge A in one window. Here we have appropriately grouped the snow drift with its parent terrain feature, and our technique would indicate the correct wind direction. If, however, we chose a 500m x 500m window that excluded ridge A and included the snow drift and adjacent ridge B, we would group the snow drift with an unrelated terrain feature. However, the technique simply looks at the relationship between terrain and snow depth and would falsely conclude that the local wind direction acts 180º from the direction that did form the drift.

We find that our correlation technique can infer the wind direction around exposed, non-vegetated ridges, and cannot infer the wind direction at sites where other processes such as forest-snow interactions dominate.

7.2 Differences in downscaling schemes as explained by model internals

The HRRR+MM and HRRR+WN wind fields tend to diverge in their predictions of wind direction in narrow concavities in the terrain (see white areas in Fig. 5, relative to DEM). To explain this result, we look to the internals of the two downscaling methods. While WindNinja may freely adjust its wind vectors without having to match forcing data at the location of the data, MicroMet is confined to interpolating its wind field between points of forcing data nodes. MicroMet then adjusts the interpolated wind direction by computing a scaling factor that accounts for local terrain curvature and slope. However, due to constraints placed on this scaling factor, the largest modification of interpolated wind direction that MicroMet can make is +/- 14.3º. If MicroMet is asked to simulate wind direction in a narrow valley, and the two closest HRRR nodes are on the valley's ridges where meso-scale wind patterns suggest a homogenous wind field, MicroMet will predict wind directions in the valley +/- 14.3º from those found on the ridges. This is a specific scenario, but it is the likely explanation for the disparity seen between MicroMet and WindNinja in narrow terrain concavities. This also explains differences in wind fields derived from different coarse datasets and downscaled using MicroMet.

A similar story is true of MicroMet's modification of wind speeds. Again, MicroMet computes a scaling factor that accounts for curvature and slope of the local terrain, then multiplies the interpolated wind field by this scaling factor. Due to constraints placed on this scaling factor, the largest modification of wind speed that MicroMet can make is 1.5 or 0.5 times the interpolated wind field. This limit results in lower wind speeds near ridgelines when compared with WindNinja. Despite this restriction on MicroMet, we find that both downscaling schemes result in more spatially heterogeneous wind speeds with greater extrema when compared to a wind field downscaled using bilinear interpolation alone (Figure 6).

These results demonstrate that MicroMet is dependent on high-resolution, accurate forcing data for computing a wind field. Modelers hoping to use MicroMet to downscale winds should ensure that they are using well-vetted weather model data of a relatively high spatial resolution, and not coarse or irregularly spaced meteorological station data.

7.3 Effect of wind fields on modeling snow depth

7.3.1 Timing of wind speeds with a variable threshold shear velocity scheme

We also investigated the timing of wind events, because our SnowModel setup used a variable threshold shear velocity [*Liston et al. 2007*]. This formulation alters the threshold shear velocity depending on time since last snowfall, density of freshly fallen snow, and wind speed. During precipitation events, the threshold shear velocity drops significantly, allowing for wind-redistribution of snow. We would also expect surface shear velocity to increase during these precipitation events, since they represent winter storms. We found that for all simulations tested, with the exception of CDEC+MM, periods of low threshold shear velocities corresponded to periods of high surface shear velocities. In other words, when the snow surface was soft and ripe for transport, these simulations had wind speeds capable of transporting it. This relationship between timing of surface shear speeds and low threshold shear speeds is expected for all of the simulations forced with HRRR winds, since HRRR precipitation is likely to overlap with HRRR winds as it models winter storms. It is notable that this overlap holds for the NLDAS+MM simulation. This simulation used the HRRR precipitation field, but NLDAS-derived winds. It demonstrates that both models predicted similar timing for the precipitation and high-wind events, and that the choice in coarse wind data may not impact the timing of surface shear exceedance when using gridded meteorological data. These results show that when using gridded model data as input to a downscaling scheme, wind-redistribution will occur as expected during winter storms. However, using observations from meteorological towers may not allow for proper timing of high wind events with precipitation events, due to sheltering of the towers by vegetation or topography.

7.3.2 Effect of spatial heterogeneity of wind speeds on wind-redistribution

To explain differences in wind-redistribution of snow between the simulations, we look to the spatial distribution of wind speeds in the forcing data. 4 of the 5 downscaled wind fields show some reflection of the local topography in the wind speed fields (Figure 6). However, the HRRR+Interp wind field, because it has not been adjusted for local topography, varies smoothly. This is significant for modeling deposition of snow via transport processes. While the HRRR+Interp simulation deposited 27% of wind-scoured snow, the average for the other 4 simulations was 87% of scoured snow being re-deposited. This is because deposition via snow transport occurs in SnowModel only when a difference in transport flux occurs. These differences in transport flux primarily occur when there are changes in wind speed, and any sharp changes in wind speed are smoothed out through the bilinear interpolation applied. Thus, in the simulations forced with wind fields downscaled with respect to terrain, snow which is scoured is typically deposited elsewhere. In the HRRR+Interp simulation, it is scoured but not deposited. Instead it remains in the atmosphere for longer and is eventually sublimated. Indeed, the HRRR+Interp simulation sees 118% of its scoured snow sublimated, while the HRRR+MM simulation sees only 38% of its scoured snow sublimated. These results demonstrate that when

modeling wind-redistribution of snow, one should apply a terrain-conscious downscaling scheme, and not simple bilinear or nearest-neighbor interpolation, to wind data.

As noted above, the NLDAS dataset draws its winds from a 32 km resolution model (NARR), and then interpolates them to the 12.5 km NLDAS grid. Since NARR runs at a 32 km resolution, it views the terrain at a coarse scale and produces a smoothed DEM. As a result, regions with tightly clustered peaks will be assigned a high mean elevation, while generally flat regions with a solitary ridge will have a mean elevation more reflective of the flats. When wind speed is calculated over these two regions, speeds will be calculated as if there are some obstacles for the clustered peaks and calculated as if there is virtually no obstacle for the lone ridge. As a result of this, the NLDAS+MM simulation achieves wind-redistribution in some mountainous areas of the modeling domain, and nearly no wind-redistribution in other sparsely mountainous areas (Figure 9). This further demonstrates that MicroMet is dependent on high-resolution, accurate forcing data.

7.4 Deposition patterns

The presence of large positive and negative biases of snow depth on the leeside of Kuna Crest seen in the HRRR+MM and HRRR+WN simulations also suggest that transported snow is being deposited in the wrong locations. Since the deposition of blowing snow occurs when there are changes in wind speed, these large biases are evidence of neither wind field capturing the true leeside wind field. The leeside wind field is characterized by large, complex eddies, which we do not expect either the HRRR+MM or HRRR+WN wind fields to resolve, especially at 150 m resolution. In fact, fully modeling leeside flow remains a challenge for even advanced CFD models [*Gerber et al. 2017*]. Prior studies have shown that model resolutions < 10 m are necessary to resolve small-scale snow features caused by wind transport, but this resolution is currently not feasible for basin-wide modeling efforts [*Mott and Lehning 2010*]. Future studies may wish to examine changes in wind speed heterogeneity, and thus deposition patterns, as model resolutions are increased from 150 m to higher resolutions. This may yield some sweet-spot in modeling resolution where the location of lee-side snow drifts is resolved without a prohibitively high model resolution.

7.5 Formulation of suspension in SnowTran

In reviewing the equations comprising SnowTran and the Prairie Blowing Snow Model's snow-redistribution schemes, we found that the primary difference between these two models comes in their calculation of transport via suspension. While they agree on the overall form of the equation, an integral of the concentration of snow in the atmosphere over the suspension layer, they disagree in their estimates of the concentration within this layer.

The method laid out in SnowModel follows a theoretical model developed for general aeolian transport of particles which considers the concentration to be determined by particle settling velocity, uplift from turbulent eddies, and the net vertical transport of particles [*Kind 1992*]. This relationship is then used to estimate the concentration at a given height, using the concentration calculated at the top of the saltation layer. The concentration equation developed for PBSM starts with the same principles governing the concentration of particles in the suspension layer [*Pomeroy and Male 1992*]. *Pomeroy and Male 1992* then introduce empirical constants derived from observations of mass concentrations throughout this layer. We found that

despite these similarities, SnowTran predicted 1-2x more transport via suspension than PBSM. Additionally, the transport rates reported by SnowModel, especially at high wind speeds, appear greater than those reported in observations [*Nishimura and Nemoto 2005; Schmidt 1982; Pomeroy and Male 1992*].

We attribute these differences to SnowTran's treatment of snow settling velocity. In their implementation of *Kind 1992*'s methodology in SnowTran, the developers of SnowTran assign a constant settling velocity for snow of 0.3 m s^{-1}, coming from *Schmidt 1982.* In Pomeroy and Male's formulation of the suspension equation, snow settling velocity is allowed to vary with particle radius. Sensitivity testing found that doubling SnowTran's settling velocity to 0.6 m s^{-1} brings its estimates of transport via suspension into agreement with PBSM and published observations [*Nishimura and Nemoto 2005; Schmidt 1982; Pomeroy and Male 1992]*. Variations of settling velocity by this amount are reported in the literature, including in the study that *Liston and Sturm 1998* cite for their 0.3 m s^{-1} estimate [*Schmidt 1982; Schmidt 1982*]. In *Schmidt 1982*, calculated snow settling velocity ranged from 0.26 to 1.05 m s^{-1} for the distribution of particle sizes observed. It is possible that the original 0.3 m s^{-1} value in SnowTran is appropriate for the colder environments that these researchers tend to study, but that this subtlety was not communicated.

While the current formulation of suspension allows for rates of transport larger than those published in observations, it is likely that SnowTran's limit on 10-m wind speeds to 30 m s^{-1} partly controls for excessive transport. However, this compensatory effect is an unsatisfying solution. The WindNinja downscaling scheme was found in this study to produce high winds and transport the most snow of all simulations tested, but this result may change if different settling velocities or blowing snow models are used. A full analysis of the settling velocity of snow and a comparison of different blowing snow models is beyond the scope of this study. Yet, considering that suspension comprises the bulk of wind-redistribution of snow (Table 3), we believe this to be worthy of future study.

8.0 Conclusion

In this study we evaluated a range of combinations of wind data and downscaling schemes for use in modeling the wind-redistribution of snow. We also introduced a new technique for inferring the wind direction at sites from the local snow depth distribution. This technique tends to be applicable at non-forested sites with median slopes between 20º and 40º. Using these inferred wind directions, we find that coarse wind data has a greater effect on wind direction than the downscaling scheme used. However, differences among downscaled wind directions tested were minor, and modeled wind direction is likely not a major source of error for modeling wind-redistribution of snow at 150 m resolutions.

We then compared downscaled wind fields directly, finding that they differ in their predictions of wind direction in narrow terrain features where the data used to force them does not provide information. This motivates the usage of relatively high-resolution (3 km) wind data for downscaling. In the narrow, forested valleys, wind speeds are usually too low for wind-transport of snow, so differences in wind direction are not important for modeling snow depth. It is possible that wind direction could be important for modeling canopy interception and unloading, but SnowModel does not include wind data in canopy processes [*Liston and Elder 2006*], and such analysis is beyond the scope of this study. The downscaling methods also

differed in their predictions of wind speed over exposed ridges. WindNinja-downscaled HRRR data reported the highest speeds over ridges, while MicroMet-downscaled HRRR data reported lower wind speeds. Implicitly, the bilinearly interpolated HRRR field did not show any speedup over ridges. These differences between WindNinja and MicroMet are explained by the internals of MicroMet, which limit how much MicroMet's predictions can deviate from the forcing data.

Results from running SnowModel with these different forcing datasets showed that wind speed distributions and spatial heterogeneity of wind speeds are the most important factors in wind forcing data. Due to the placement of the wind sensors, CDEC+MM simulations did not achieve high enough wind speeds to allow for wind-redistribution of snow. NLDAS+MM simulations had inconsistent performance across the basin, since NLDAS wind data come from a model which views the terrain at a 32 km resolution. The MM-downscaled and bilinearly interpolated HRRR data had similar distributions of wind speed, but the homogeneity of the interpolated HRRR data resulted in decreased deposition of transported snow and thus increased sublimation. Lastly, the HRRR+WN simulation predicted wind speeds greater than 60 m s^{-1} at 10-m height over exposed ridges, leading to the most wind-redistribution of snow of all of the simulations run.

These results lead us to conclude that, in order to model wind-redistribution of snow, snow modelers should downscale wind data from weather models. These weather models should be of a reasonably high-resolution 3 km and the downscaling scheme should account for local topography. We find that downscaling 3 km HRRR data with the MicroMet scheme achieves this.

In the process of this work, we also discovered two components of the SnowTran model worthy of further review. The first being its treatment of transport flux out of areas downwind of forested grid cells, and the second being its treatment of snow settling velocity as a constant when calculating transport via suspension. Improvements should be made to the suspension scheme in SnowTran so that it considers the settling velocity of snow grains as variable. Regardless of these issues, SnowTran has proven to be a useful tool for recreating snow depth distribution patterns when compared to simulations without it.

Future studies using correlation analysis to infer wind direction should test it in on high-resolution LiDAR data to investigate whether this technique works across different length scales. As regular LiDAR scans of snow depth increase in resolution into the sub-meter domain, fine-scale patterns of wind and snow interaction such as sastrugi and barchans can be used to infer wind direction. Additionally, taking the cross-correlation of snow depth with vegetation height as well as snow depth with terrain may increase the range of sites at which this technique is applicable. Future studies should also look at whether snow depth output from snow models forced with empirically- or physically-based downscaling schemes diverge at higher modeling resolutions. This would determine at what modeling resolution it is necessary to use more physically explicit downscaling schemes of winds.

Bibliography

Beaucage, P., Brower, M. C., & Tensen, J. (2014). Evaluation of four numerical wind flow models for wind resource mapping. *Wind Energy*, *17*, 197–208. https://doi.org/10.1002/we.1568

Becker, R. A., Tikoff, B., Riley, P. R., & Iverson, N. R. (2014). Preexisting fractures and the formation of an iconic American landscape: Tuolumne Meadows, Yosemite National Park, USA. *GSA Today*, *24*(11), 4–10. https://doi.org/10.1130/GSATG203A.1

Benjamin, S. G., Weygandt, S. S., Brown, J. M., Hu, M., Alexander, C. R., Smirnova, T. G., … Manikin, G. S. (2015). A North American Hourly Assimilation and Model Forecast Cycle: The Rapid Refresh. *Monthly Weather Review*, *144*(4), 1669–1694. https://doi.org/10.1175/mwr-d-15-0242.1

Blaylock, B. K., Horel, J. D., & Liston, S. T. (2017). Cloud archiving and data mining of High-Resolution Rapid Refresh forecast model output. *Computers and Geosciences*, *109*(July), 43–50. https://doi.org/10.1016/j.cageo.2017.08.005

Currier, W. R., Pflug, J., Mazzotti, G., Jonas, T., Deems, J. S., Bormann, K. J., … Lundquist, J. D. (2019). Comparing Aerial Lidar Observations With Terrestrial Lidar and Snow-Probe Transects From NASA's 2017 SnowEx Campaign. *Water Resources Research*, 6285–6294. https://doi.org/10.1029/2018WR024533

Currier, W. R., & Lundquist, J. D. (2018). Snow Depth Variability at the Forest Edge in Multiple Climates in the Western United States. *Water Resources Research*, *54*(11), 8756–8773. https://doi.org/10.1029/2018WR022553

Deems, J. S., Fassnacht, S. R., & Elder, K. J. (2006). Fractal Distribution of Snow Depth from Lidar Data. *Journal of Hydrometeorology*, *7*(2), 285–297. https://doi.org/10.1175/jhm487.1

Deems, J. S., Fassnacht, S. R., & Elder, K. J. (2008). Interannual Consistency in Fractal Snow Depth Patterns at Two Colorado Mountain Sites. *Journal of Hydrometeorology*, *9*(5), 977–988. https://doi.org/10.1175/2008jhm901.1

Filhol, S., & Sturm, M. (2015). Snow bedforms: A review, new data, and. *Journal of Geophysical Research: Earth Surface*, *120*, 1645–1669. https://doi.org/10.1002/2015JF003529.Received

Forthofer, J. M., Butler, B. W., & Wagenbrenner, N. S. (2014). A comparison of three approaches for simulating fine-scale surface winds in support of wildland fire management.

Part I. Model formulation and comparison against measurements. *International Journal of Wildland Fire*, *23*(7), 969–981. https://doi.org/10.1071/WF12089

Gascoin, S., Lhermitte, S., Kinnard, C., Bortels, K., & Liston, G. E. (2013). Wind effects on snow cover in Pascua-Lama, Dry Andes of Chile. *Advances in Water Resources*, *55*, 25–39. https://doi.org/10.1016/j.advwatres.2012.11.013

Gerber, F., M. Lehning, S. W. Hoch, and R. Mott (2017), A close-ridge small-scale atmospheric flow field and its influence on snow accumulation, J. Geophys. Res. Atmos., 122, 7737–7754, doi:10.1002/2016JD026258.

Grayson, R., and G. Blöschl (2001), Spatial Patterns in Catchment Hydrology: Observations and Modelling, Cambridge Univ. Press, Cambridge, U. K.

Horvath, K., Koracin, D., Vellore, R., Jiang, J., & Belu, R. (2012). Sub-kilometer dynamical downscaling of near-surface winds in complex terrain using WRF and MM5 mesoscale models. *Journal of Geophysical Research Atmospheres*, *117*(11), 1–19. https://doi.org/10.1029/2012JD017432

Kind, R. J. (1992). One-dimensional aeolian suspension above beds of loose particles-A new concentration-profile equation. *Atmospheric Environment Part A, General Topics*, *26*(5), 927–931. https://doi.org/10.1016/0960-1686(92)90250-O

Lehning, M., I. Völksch, D. Gustafsson, T. A. Nguyen, M. Stähli, and M. Zappa, 2006: ALPINE3D: A detailed model of mountain surface processes and its application to snow hydrology. *Hydrol. Processes*, **20**, 2111–2128, doi:https://doi.org/10.1002/hyp.6204.

Li, L., & Pomeroy, J. W. (1997). Estimates of Threshold Wind Speeds for Snow Transport Using Meteorological Data. *Journal of Applied Meteorology*, *36*(3), 205–213. https://doi.org/10.1175/1520-0450(1997)036<0205:eotwsf>2.0.co;2

Liston, G. E., & Elder, K. (2006). A Meteorological Distribution System for High-Resolution Terrestrial Modeling (MicroMet). *Journal of Hydrometeorology*, *7*(2), 217–234. https://doi.org/10.1175/jhm486.1

Liston, G. E., Haehnel, R. B., Sturm, M., Hiemstra, C. A., Berezovskaya, S., & Tabler, R. D. (2007). Simulating complex snow distributions in windy environments using SnowTran-3D. *Journal of Glaciology*, *53*(181), 241–256. https://doi.org/10.3189/172756507782202865

Liston, G. E., & Sturm, M. 1998: A snow-transport model for complex terrain. J. Glaciol., 44, 498–516.

Luce, C. H., Tarboton, D. G., & Cooley, K. R. (1998). The influence of the spatial distribution of snow on basin-averaged snowmelt. *Hydrological Processes*, *12*(10–11), 1671–1683. https://doi.org/10.1002/(SICI)1099-1085(199808/09)12:10/11<1671::AID-HYP688>3.0.CO;2-N

Lundquist, J. D., Dettinger, M. D., & Cayan, D. R. (2005). Snow-fed streamflow timing at different basin scales: Case study of the Tuolumne River above Hetch Hetchy, Yosemite, California. *Water Resources Research*, *41*(7), 1–14. https://doi.org/10.1029/2004WR003933

Lundquist, J. D., Hughes, M., Henn, B., Gutmann, E. D., Livneh, B., Dozier, J., & Neiman, P. (2015). High-elevation precipitation patterns: Using snow measurements to assess daily gridded datasets across the Sierra Nevada, California. *Journal of Hydrometeorology*, *16*(4), 1773–1792. https://doi.org/10.1175/JHM-D-15-0019.1

Margulis, S. A., Cortés, G., Girotto, M. & Durand, M. (2016). A Landsat-Era Sierra Nevada snow reanalysis (1985–2015). *Journal of Hydrometeorology.* **17**(4), 1203–1221, https://doi.org/10.1175/JHM-D-15-0177.1

Marks, D., & Winstral, A. (2002). Comparison of Snow Deposition, the Snow Cover Energy Balance, and Snowmelt at Two Sites in a Semiarid Mountain Basin. *Journal of Hydrometeorology*, *2*(3), 213–227. https://doi.org/10.1175/1525-7541(2001)002<0213:cosdts>2.0.co;2

Mott, R., Schirmer, M., & Lehning, M. (2011). Scaling properties of wind and snow depth distribution in an Alpine catchment. *Journal of Geophysical Research Atmospheres*, *116*(6), 1–8. https://doi.org/10.1029/2010JD014886

Mott, R., Vionnet, V., & Grünewald, T. (2018). The Seasonal Snow Cover Dynamics: Review on Wind-Driven Coupling Processes. *Frontiers in Earth Science*, *6*(December). https://doi.org/10.3389/feart.2018.00197

Mott, R., and Lehning, M. (2010). Meteorological modeling of very high resolution wind fields and snow deposition for mountains. J. Hydromet. 11, 934–949. doi: 10.1175/2010JHM1216.1

Musselman, K. N., Pomeroy, J. W., Essery, R. L. H., & Leroux, N. (2015). Impact of windflow calculations on simulations of alpine snow accumulation, redistribution and ablation. *Hydrological Processes*, *29*(18), 3983–3999. https://doi.org/10.1002/hyp.10595

Nishimura, K., & Nemoto, M. (2005). Blowing snow at Mizuho station, Antarctica. *Philosophical Transactions of the Royal Society A: Mathematical, Physical and Engineering Sciences*, *363*(1832), 1647–1662. https://doi.org/10.1098/rsta.2005.1599

Ohara, N. (2014). Water Resources Research. *Journal of the American Water Resources Association*, *5*(3), 2–2. https://doi.org/10.1111/j.1752-1688.1969.tb04897.x

Painter, T. H., Berisford, D. F., Boardman, J. W., Bormann, K. J., Deems, J. S., Gehrke, F., … Winstral, A. (2016). The Airborne Snow Observatory: Fusion of scanning lidar, imaging spectrometer, and physically-based modeling for mapping snow water equivalent and snow albedo. *Remote Sensing of Environment*, *184*, 139–152. https://doi.org/10.1016/j.rse.2016.06.018

Pflug, J. M., Liston, G. E., Nijssen, B., & Lundquist, J. D. (2019). Testing Model Representations of Snowpack Liquid Water Percolation Across Multiple Climates. *Water Resources Research*, 4820–4838. https://doi.org/10.1029/2018WR024632

Pomeroy, J. W., Gray, D. M., & Landine, P. G. (1993). The Prairie Blowing Snow Model: characteristics, validation, operation. *Journal of Hydrology*, *144*(1–4), 165–192. https://doi.org/10.1016/0022-1694(93)90171-5

Pomeroy, J. W., Marsh, P., & Gray, D. M. (1997). Application of a distributed blowing snow model to the Arctic. *Hydrological Processes*, *11*(11), 1451–1464. https://doi.org/10.1002/(sici)1099-1085(199709)11:11<1451::aid-hyp449>3.3.co;2-h

Pomeroy, J. W., & Male, D. H. (1992). Steady-state suspension of snow. *Journal of Hydrology*, *136*(1–4), 275–301. https://doi.org/10.1016/0022-1694(92)90015-N

Raleigh, M. S., Livneh, B., Lapo, K., & Lundquist, J. D. (2016). How does availability of meteorological forcing data impact physically based snowpack simulations? *Journal of Hydrometeorology*, *17*(1), 99–120. https://doi.org/10.1175/JHM-D-14-0235.1

Riley, P., & Tikoff, B. (2010). Tabular fracture clusters: Dynamic fracturing produced by volatile expulsion, Sierra Nevada Batholith, California. *Journal of Structural Geology*, *32*(10), 1488–1499. https://doi.org/10.1016/j.jsg.2010.09.006

Schmidt, R. A. (1982). Properties of blowing snow. *Reviews of Geophysics*, *20*(1), 39–44. https://doi.org/10.1029/RG020i001p00039

Schmidt. R. A. (1982). Vertical profiles of wind speed, snow concentration and humidity in blowing snow. *Boundary-Layer Meteorol*., 23(2), 223-246.

Shean, D. E., Alexandrov, O., Moratto, Z. M., Smith, B. E., Joughin, I. R., Porter, C., & Morin, P. (2016). An automated, open-source pipeline for mass production of digital elevation models (DEMs) from very-high-resolution commercial stereo satellite imagery. *ISPRS Journal of Photogrammetry and Remote Sensing*, *116*(206), 101–117. https://doi.org/10.1016/j.isprsjprs.2016.03.012

Sturm, M., & Wagner, A. M. (2010). Using repeated patterns in snow distribution modeling: An Arctic example. *Water Resources Research*, *46*(12), 1–15. https://doi.org/10.1029/2010WR009434

Wagenbrenner, N. S., Forthofer, J. M., Lamb, B. K., Shannon, K. S., & Butler, B. W. (2016). Downscaling surface wind predictions from numerical weather prediction models in complex terrain with WindNinja. *Atmospheric Chemistry and Physics*, *16*(8), 5229–5241. https://doi.org/10.5194/acp-16-5229-2016

Winstral, A., Elder, K., & Davis, R. E. (2002). Spatial Snow Modeling of Wind-Redistributed Snow Using Terrain-Based Parameters. *Journal of Hydrometeorology*, *3*(5), 524–538. https://doi.org/10.1175/1525-7541(2002)003<0524:ssmowr>2.0.co;2

Xia, Y., Mitchell, K., Ek, M., Sheffield, J., Cosgrove, B., Wood, E., … Mocko, D. (2012). Continental-scale water and energy flux analysis and validation for the North American Land Data Assimilation System project phase 2 (NLDAS-2): 1. Intercomparison and application of model products. *Journal of Geophysical Research Atmospheres*, *117*(3). https://doi.org/10.1029/2011JD016048

Yang, L., Jin, S., Danielson, P., Homer, C.G., Gass, L., Bender, S.M., Case, A., Costello, C., Dewitz, J.A., Fry, J.A., Funk, M., Granneman, B.J., Liknes, G.C., Rigge, M.B., and Xian, G., 2018, A new generation of the United States National Land Cover Database—Requirements, research priorities, design, and implementation strategies: ISPRS Journal of Photogrammetry and Remote Sensing, v. 146, p. 108–123, at https://doi.org/10.1016/j.isprsjprs.2018.09.006.

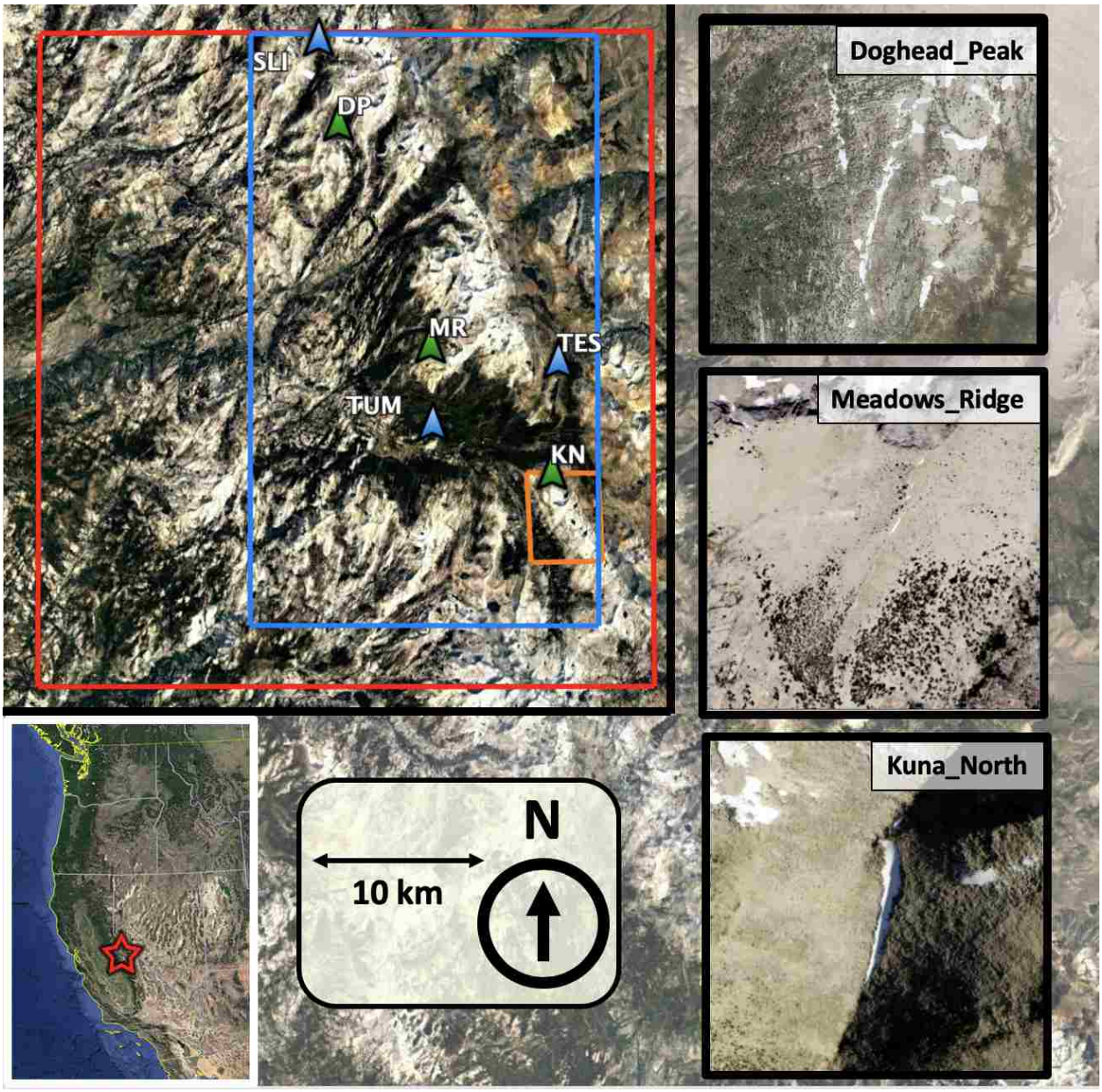

Figure 1: Map of study area in Tuolumne Meadows, CA. The red perimeter shows the area over which wind fields were calculated and compared with inferred wind directions. The blue perimeter shows the area over which SnowModel was run. The orange perimeter shows the area referred to as Kuna Crest in sections 6 and 7. Note that the legend and scale bar indicate the scale of the domain shown in the upper left and is not representative of the scale at the three sites shown on the right. The blue arrows show the locations of CDEC meteorological towers, labeled by their reference names on CDEC. The green arrows indicate the locations of the three sites shown on the right, where snow drifts were identified from late-lying snow near ridgelines.

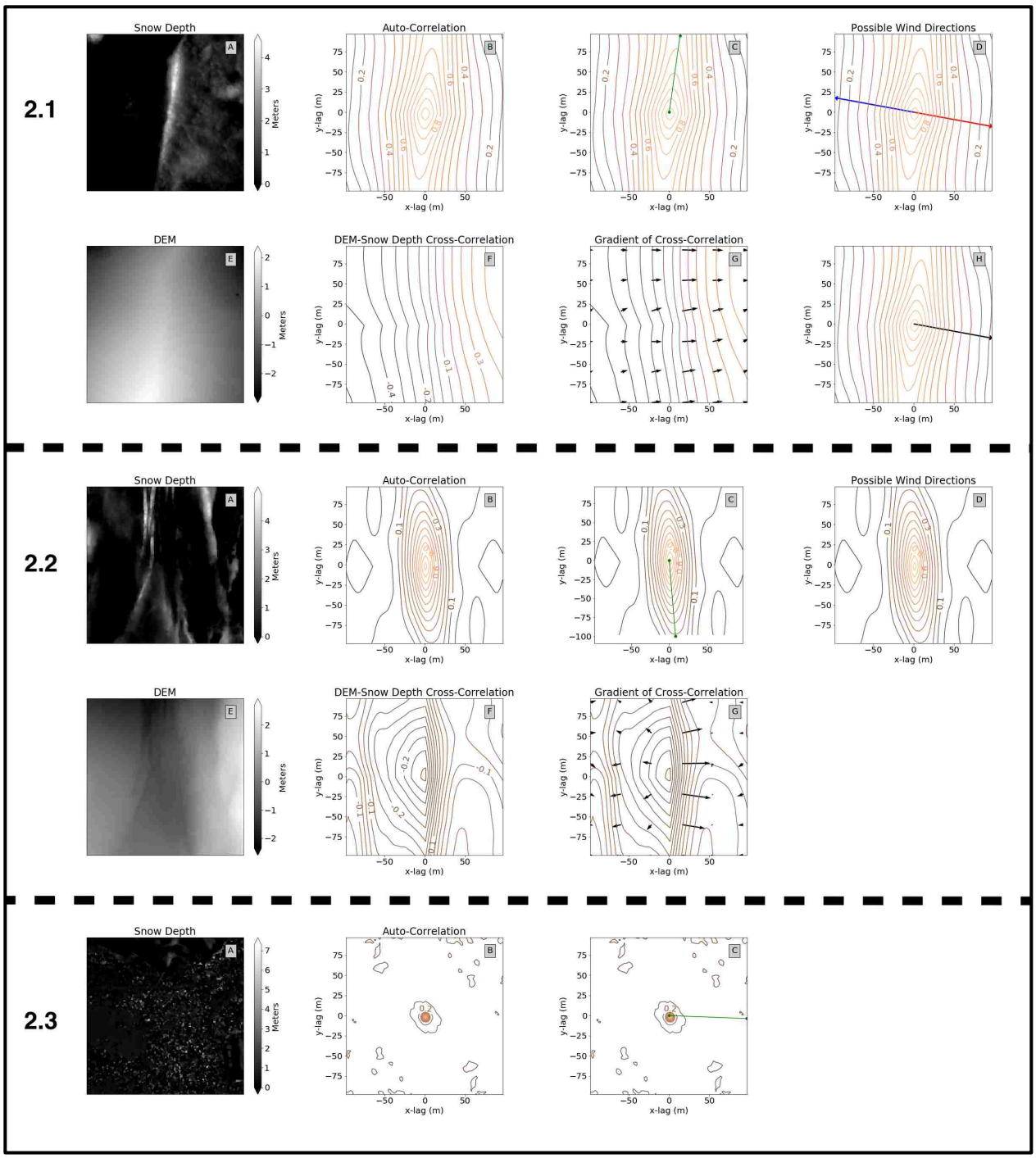

Figure 2: The process used to infer the wind direction at a 500 x 500m site. Warmer colors on the contour plots indicate contours of high correlation values. 2.1 shows a successful inference at Kuna_North. 2.2 shows an unsuccessful inference due to disagreement in the gradient of the cross-correlation. 2.3 shows an unsuccessful inference due to a lack of an anisotropy in the autocorrelation function.

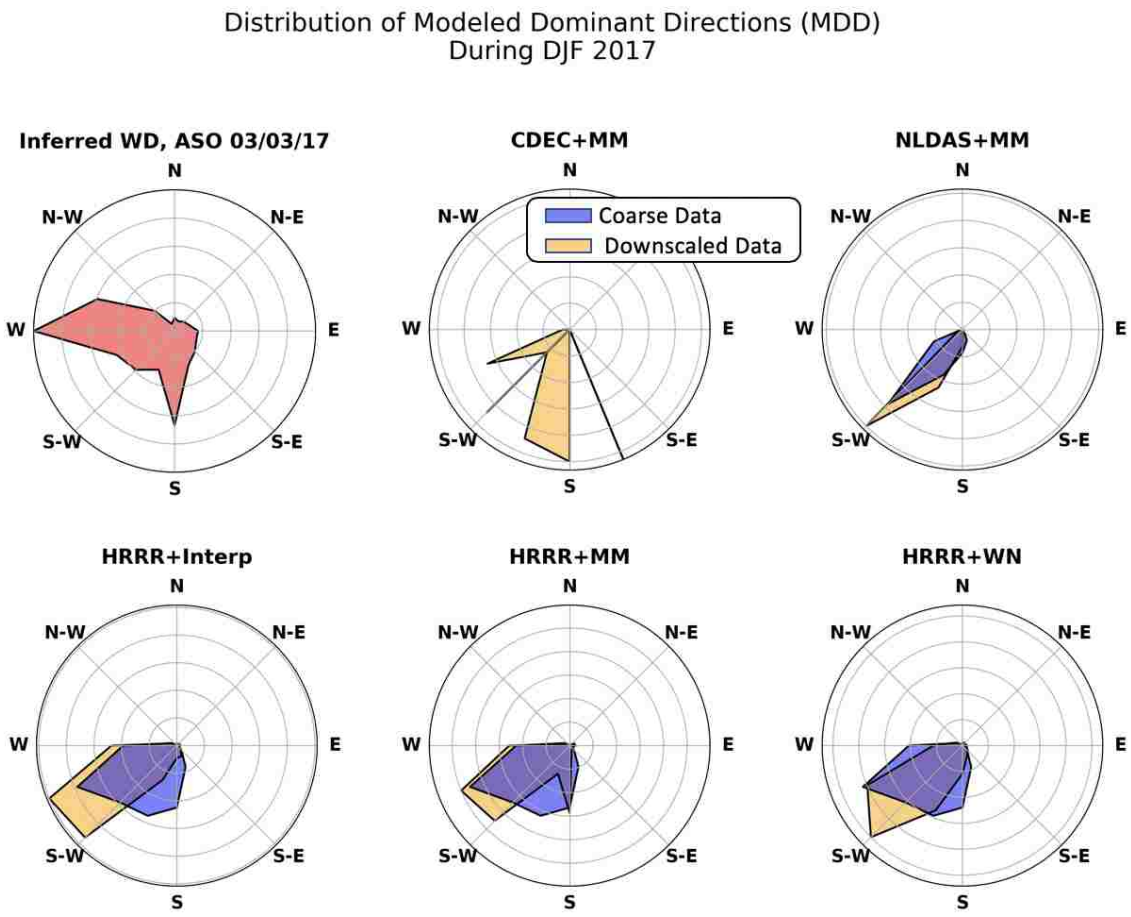

Figure 3: Comparison of coarse and downscaled wind direction distributions compared to the distribution of inferred wind directions. The distributions shown are normalized PDFs of the wind direction. This means that the area of each distribution is not indicative of the total number of data points that it contains. This is done so that all distributions, including the narrowly distributed coarse CDEC data, are visible here. Windrose titles refer to the wind field used, in the format "Coarse_Data+Downscaling_Method".

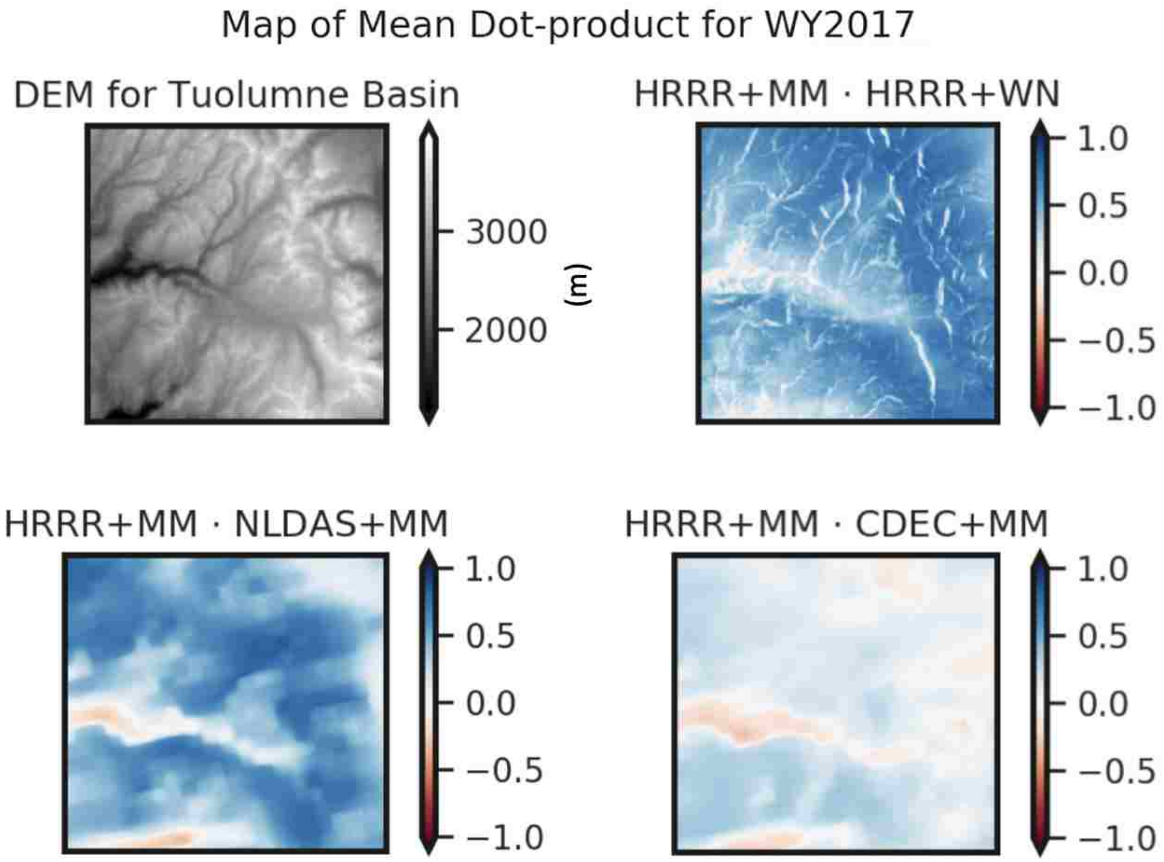

Figure 4: Spatial comparison of the mean dot-products between wind vectors of different wind fields for WY2017. Wind field vectors are normalized before the dot-product is taken so that only the modeled wind directions are compared. Regions of value 1 indicate agreement between the wind fields on the wind direction, whereas regions of value -1 indicate disagreement.

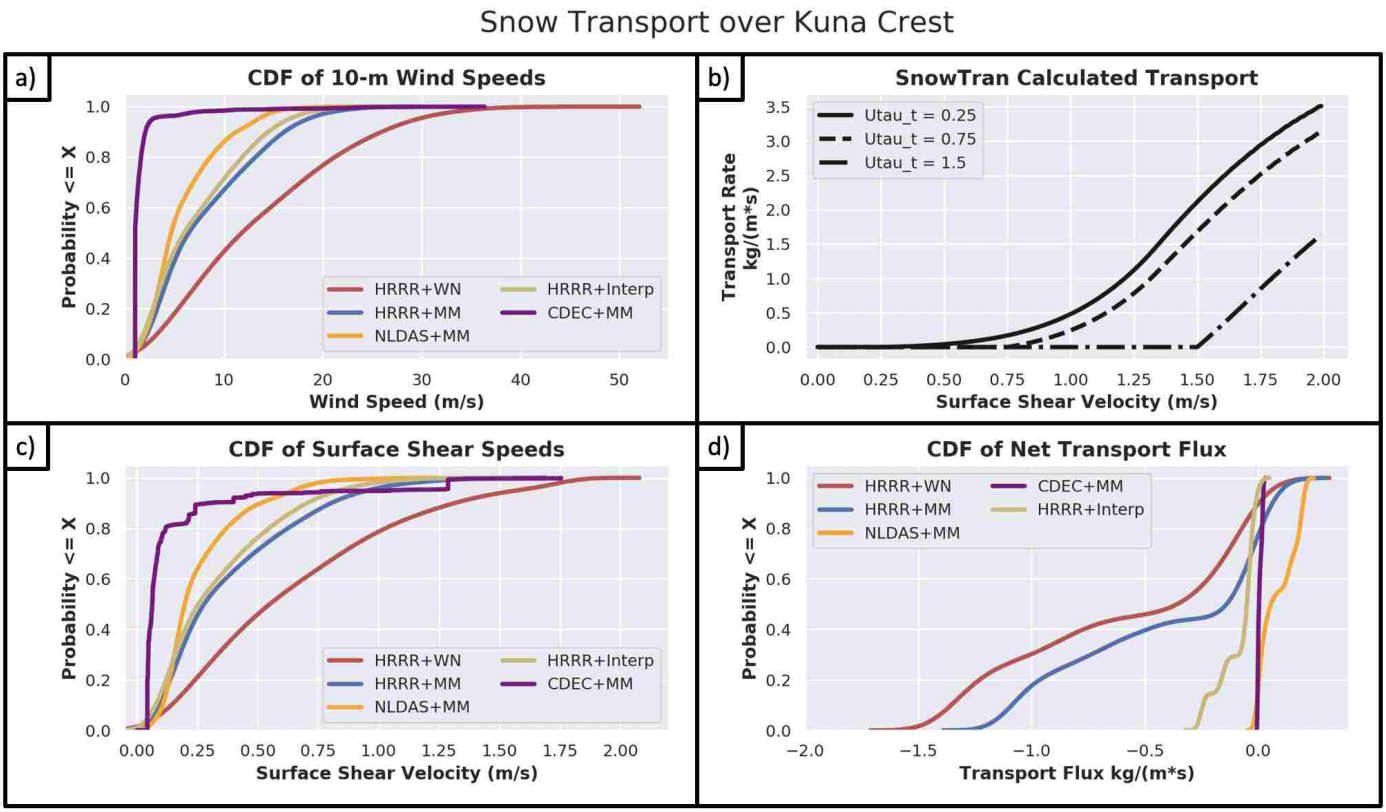

Figure 5: Wind speeds and net snow transport fluxes for a SnowModel grid cell on Kuna Crest for Oct 2016 – April 2017. Panel a) shows cumulative distribution functions (CDFs) of 10-m wind speeds as ingested by SnowModel. Panel b) shows SnowTran's calculated transport rate as a function of surface shear velocity. Panel c) shows CDFs for the surface shear speeds modeled by SnowModel. Panel d) shows a CDF of net transport fluxes. Negative fluxes indicate net scouring of snow from the grid cell, positive fluxes indicate net deposition of snow to the grid cell.

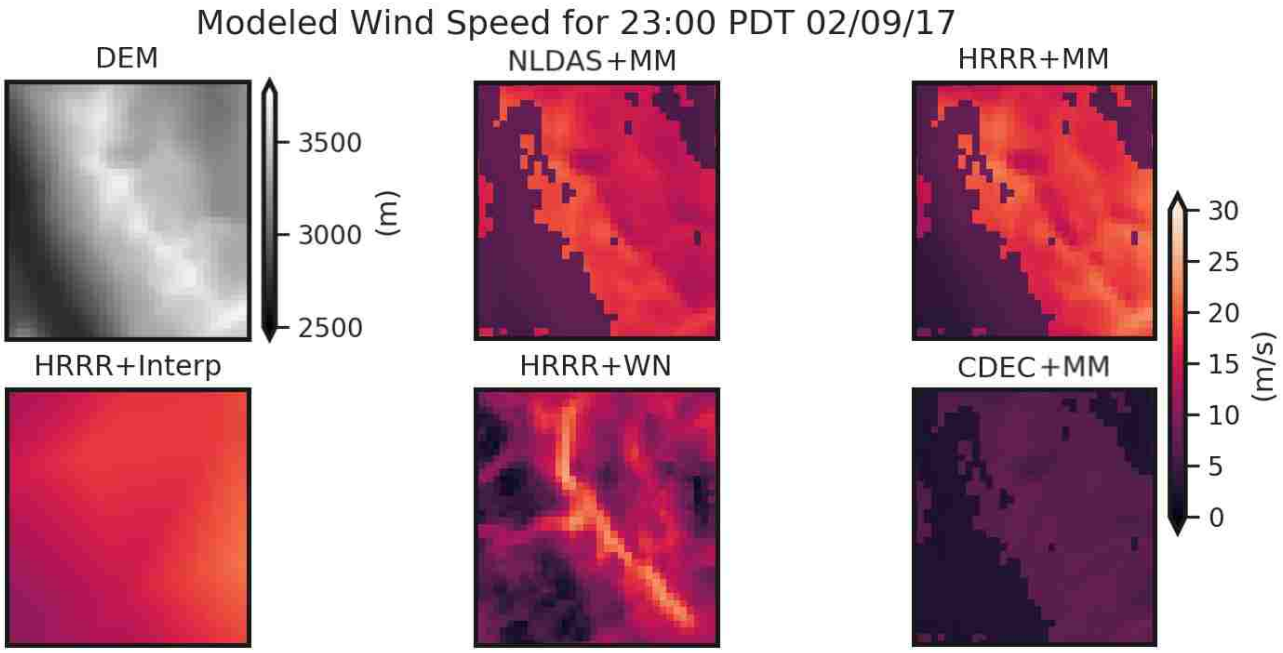

Figure 6: Spatial comparison of wind speeds over Kuna Crest. The time shown was selected as it was a high-wind event where spatial differences between the wind fields are most apparent for demonstrative purposes. The abrupt change in speeds in the MicroMet downscaled wind fields corresponds to a transition from forested to non-forested grid cells.

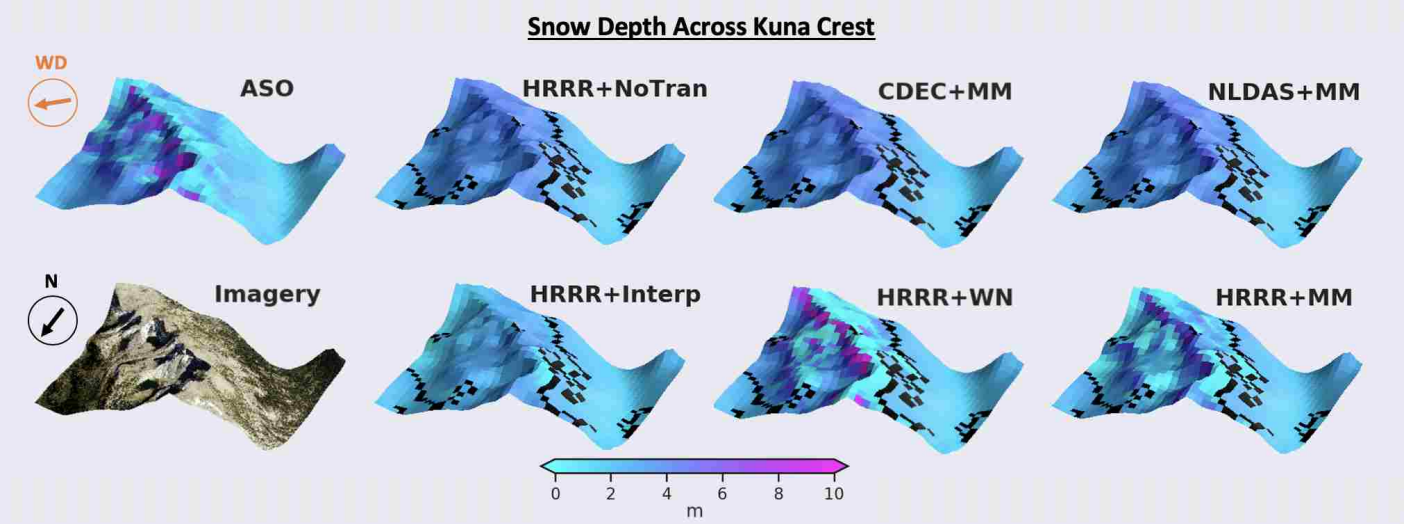

Figure 7: Map of the spatial distributions of modeled snow depth across Kuna Crest for all SnowModel simulations. The area shown spans 5.25 km x 5.25 km. ASO data comes from the 04/01/2017 flight. Imagery comes from the NAIP program. The arrow labeled "WD" shows the dominant wind direction across this ridge, and the arrow labeled "N" indicates the direction of North. Note the presence of deep snow drifts in the HRRR+WN and HRRR+MM simulation that are also observed in ASO data. The black pixels correspond to non-forested grid cells downwind of forested grid cells, which were masked out as discussed in Section 4.2.

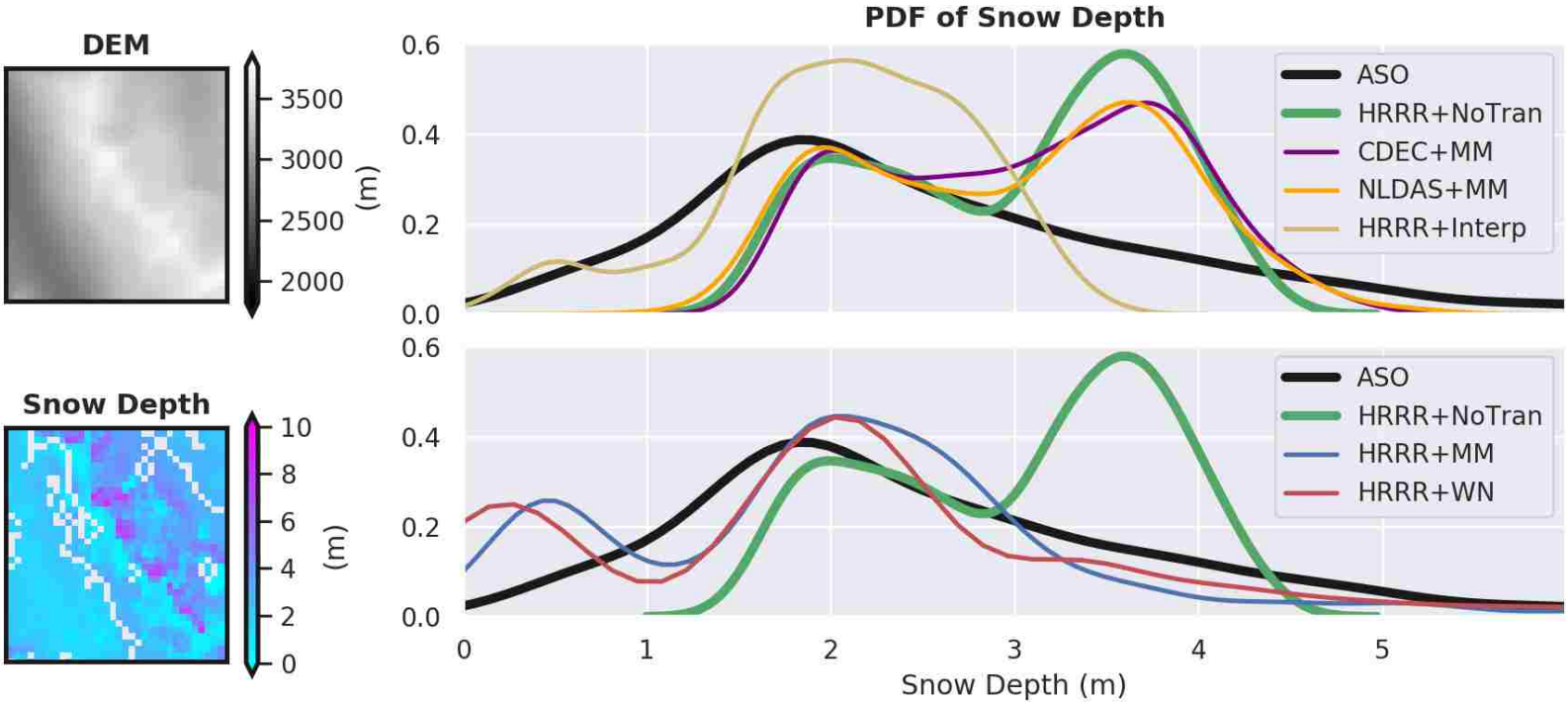

Figure 8: PDFs of the snow depth distributions across Kuna Crest for each SnowModel configuration shown in figure 7. The SnowModel simulations which use the CDEC+MM and NLDAS+MM wind fields to calculate wind transport of snow result in distributions similar to the simulation run without wind transport of snow. The simulation forced with the HRRR+Interp wind field produced a distribution with more low snow depth values and fewer high snow depth values when compared to observations from ASO. The SnowModel simulations which used the HRRR+WN and HRRR+MM wind fields best matched the distribution of snow depth values captured by observations.

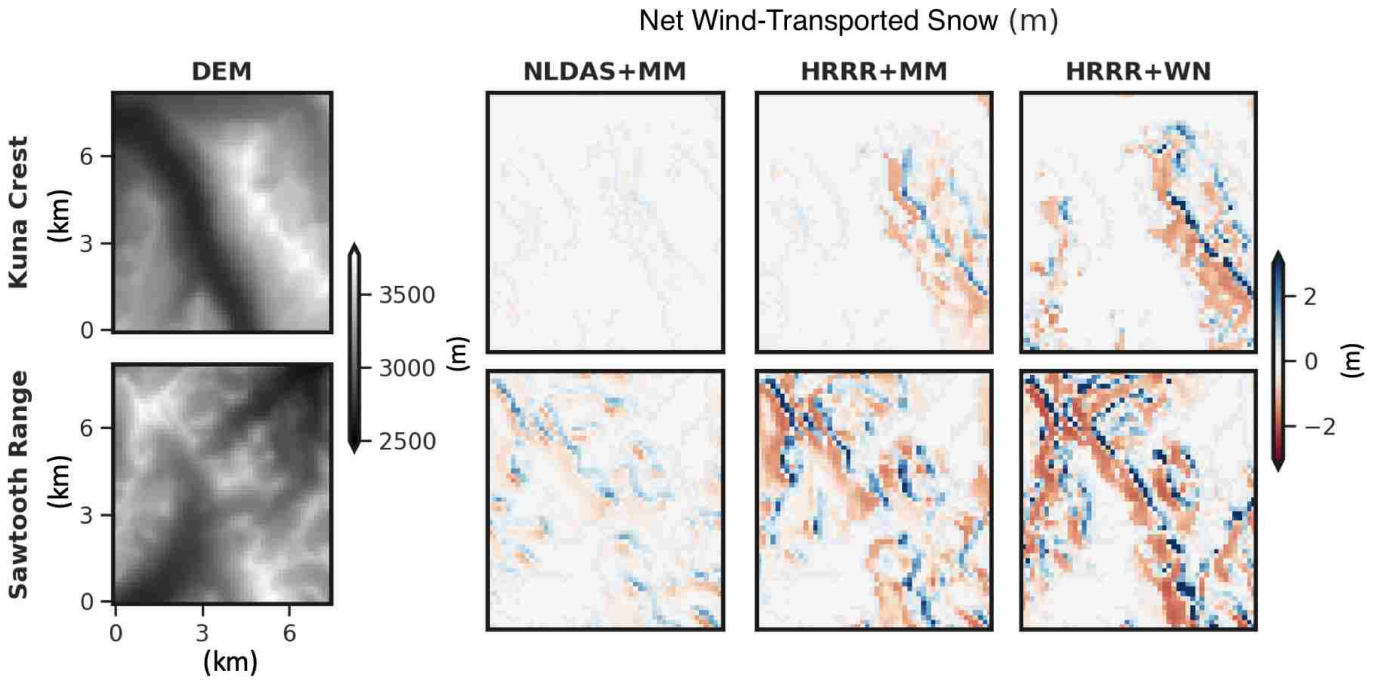

Figure 9: Spatial distribution of modeled net wind-transport of snow at two different sites. Map of accumulated snow transported in three simulations due to saltation and suspension. The top row shows net wind-transport over Kuna Crest, while the bottom row shows net wind-transport over Sawtooth Range. Net wind-transport is calculated as the sum of saltation and suspension. At both locations, the SnowModel simulation forced with the HRRR+WN wind field produces the most wind-transport of snow compared to the NLDAS+MM and HRRR+MM forced simulations. Over Kuna Crest, a ridgeline with local prominence, The NLDAS+MM forced simulation produced less net wind-transport than the HRRR+MM and HRRR+WN simulations. Over the Sawtooth Range, which is in a more mountainous region, the NLDAS+MM forced simulation produced net wind-transport totals more similar to those in the HRRR+MM and HRRR+WN simulations

SnowModel Configuration	Forcing data (P, T, RH)	Wind data (WS, WD)	Downscaling	SnowTran
HRRR+NoTran	HRRR nodes	HRRR nodes	MicroMet	Off
HRRR+Interp	HRRR nodes	HRRR nodes	Bilinear-interpolation	On
HRRR+MM	HRRR nodes	HRRR nodes	MicroMet	On
HRRR+WN	HRRR nodes	WindNinja	WindNinja	On
NLDAS+MM	HRRR nodes	NLDAS nodes	MicroMet	On
CDEC+MM	HRRR nodes	CDEC Stations	MicroMet	On

Table 1. Configurations of the six SnowModel Simulations

	Percent of all Sites	Mode Site Vegetation Type	Mean Site Slope (º)	Mean Site Elevation (m)
WD Could Be Inferred	8%	Bare	23	3100
WD Could Not Be Inferred	92%	Forested	20	2800
	Number of Inferred WD	**Bare Vegetation Type**	**Slopes Between 20º-40º**	**Elevation above 3100 m**
Study Domain	260	30%	48%	20%

Table 2. Characteristics of sites where inferences of wind direction were attempted. Vegetation type of a site is determined by the mode of the vegetation type over the site. Elevation and Snow Depth for a site are calculated as the mean over the site. Slope is the median slope calculated from the 3m DEM over the site.

SnowModel Configuration	Bias, Whole Domain (cm)	Bias, Kuna Crest (cm)	Cell-mean static sublimation (cm)	Cell-mean blowing sublimation (cm)	Cell-mean Suspension Deposition (cm)	Cell-mean Saltation Deposition (cm)	Cell-mean Suspension Scour (cm)	Cell-mean Saltation Scour (cm)	Threshold Shear Speed Exceedance %
HRRR+NoTran	19	48	6	N/A	N/A	N/A	N/A	N/A	N/A
HRRR+Interp	-21	-35	8	13	3	0	-10	-1	46
HRRR+MM	-16	-30	6	13	34	2	-31	-3	51
HRRR+WN	-24	-21	8	13	46	3	-50	-4	51
NLDAS+MM	11	53	4	5	16	1	-15	-2	42
CDEC+MM	28	58	1	1	2	0	-4	0	28

Table 3. Statistics from the SnowModel simulations. All values reported in cm of SWE. Biases are computed relative to ASO data. "Cell-mean" refers to the total quantities averaged across all grid cells in the domain